Ruyong Formula (RYF) Attenuates the Abnormal Phenotypic Changes of Thymic Epithelial Cells in 4T1 Breast Cancer Mice

Bing-Qian He
Zhejiang Chinese Medical University https://orcid.org/0000-0002-0176-6011
Rong-Zhen Shi
Zhejiang Chinese Medical University
Qi-han Luo
Zhejiang Chinese Medical University
Wen-Qin Guo
Zhejiang Chinese Medical University
Xie Xu
Zhejiang Chinese Medical University
Kai He
Zhejiang University School of Medicine First Affiliated Hospital
Jian-Li Gao (jianligao@zcmu.edu.cn)
Zhejiang Chinese Medical University

Research

Keywords: RYF, thymus epithelial cells, TGF-β1, phenotypic changes, breast cancer

Posted Date: June 11th, 2021

DOI: https://doi.org/10.21203/rs.3.rs-591139/v1

Abstract

Background

Epithelialization of the breast epithelial cell is the critical step in breast cancer, but the phenotypic changes of thymus epithelial cells (TEC) and the following immune abnormalities during the development of breast cancer are rarely examined. Ruyong Formula (RYF) has been used for thousands of years, our previous researches have shown it could attenuates atrophied thymic epithelial tissue in breast cancer mice, but the mechanism is still unknown.

Methods

HPLC was used to analyze the chemical components of RYF. The 4T1 breast cancer mice model was established to study the anticancer effects of RYF. The efficacy of RYF on tumor volume, anti-tumor rate and organ index were observed. The thymus tissue were stained with Hematoxylin-Eosin (H&E) to observe the morphological changes. Cell phenotype marker, such as E-cadherin, α-tubulin and Vimentin were observed by immunofluorescence staining in TGF-β1-induced iTECs after RYF treatment. The mRNA levels of phenotypic markers and phenotype-related transcription factors, including E-cadherin, Vimentin, Zeb-1, Snail 1 and Smad 2 were detected by qPCR. The effect of RYF on the activation of Smad pathway in TGF-β1 induced iTECs was detected by luciferase reporter assay.

Results

RYF could reduce the metastatic rate and the number of pulmonary metastases in breast cancer mice and increased anti-tumor rates. Compared with the thymus in normal group, RYF increased the number of thymocytes in the cortex regions. In vitro study indicated the EMT promotion effect of TGF-β1, shown as the decreasing of E-cadherin and up-regulation of the Vimentin's expression. The level of Snail 1 and Zeb 1 increased significantly, and the mRNA levels of Smad 2 was up-regulated. Compared with TGF-β1 group, RYF-treated TECs reversed the proteins expression of E-cadherin and Vimentin and the mRNA levels of Snail 1 and Zeb 1. RYF also promoted the proliferation of iTECs, and confronted the TGF-β1 induced phenotypic transition in iTECs.

Conclusion

The abnormal thymic function of breast cancer mice was mainly due to the disorder of cortex and medulla regions cells and the atrophy of cortex. Interestingly, RYF could reverse the phenotypic changes of TECs in breast cancer by inhibiting the TGF-β1/Smad pathway.

Background

Worldwide, breast cancer is the most common cancer affecting women and remains a major health problem. It is an aggressive disease with approximately 17 million new cases each year [1]. However, there is still no gold standard treatment for metastatic breast cancer, such as triple-negative breast

cancer, so far in spite of great improvements have been made in detection and diagnosis [2]. Especially the patients of advanced breast cancer, the tumor microenvironment and chemoradiotherapy for patients with malignant diseases often lead to serious immune and hematopoietic system damage. Immunologic dysfunction, which is difficult for patients to recover from trauma, cachexia and other problems, seriously affect the survival and survival rate of patients. However, for patients with advanced breast cancer, there is no recognized treatment methods at present.

Medicinal herbs, such as Traditional Chinese Medicine (TCM), have been used as an adjunct treatment for improving the quality of life in cancer patients and exhibit potential anti-cancer activity against various type cancer including breast cancer [3]. And there are other research under way on the treatment of cancer by TCM [4–5]. *Ruyong Formula* (RYF) has been used for thousands of years, with the earliest description being recorded in 1481 in *"dan xi xin fa"*, (recorded the clinical experiences and prescriptions of Zhu Danxi, a famous doctor of Yuan Dynasty in China). It is composed of Radix Codonopsis, Astragalus membranaceus, Angelica Sinensis, Radix Bupleuri, Rhizoma Chuanxiong, raw Radix Paeoniae Alba, Fructus Forsythiae, Radix Glycyrrhizae, Trichosanthes kirilowii Maxim and Pericarpium Citri Reticulatae Viride. Pharmacological studies have showed that the Radix Codonopsis, Astragalus membranaceus and Angelica Sinensis in RYF have effective therapeutic effect in anti-inflammatory, anti-tumor, immunity enhancement and so on [6–10]. Meanwhile, the extract of Radix Codonopsis[11], Astragalus membranaceus [12, 13], Angelica Sinensis[14], raw Radix Paeoniae Alba[15], Fructus Forsythiae[16] and Trichosanthes kirilowii Maxim[17] could inhibit EMT (epithelial–mesenchymal transition), which is an important development process of cell adhesion and migration. Our primary study shown that Ruyong Formula influence the phenotypic changes of thymic epithelial cells in 4T1 breast cancer mice, but the mechanisms of action and its effect on mouse breast cancer metastasis are still unknown[18].

In this study, we explored the effect and mechanism of action of RYF on phenotypic changes of thymic epithelial cells in breast cancer mice. We studied the changes of anti-tumor rate, pulmonary metastasis, thymus histopathology features and related proteins expression (E-acdherin, Vimentin) in 4T1 breast cancer mice after RYF treated in vivo. We evaluated whether RYF could influence the proliferation and reverse the phenotypic changes caused by TGF-β1 in iTECs in vitro. We also examined the change of TGFβ/Smad pathway related to the EMT process.

Materials And Methods

Aqueous extract preparation and high performance liquid chromatography (HPLC) analysis

Ruyong formula (RYF) is composed of Radix Codonopsis (15g), Astragalus membranaceus (20g), Angelica Sinensis (12g), Radix Bupleuri (12g), Rhizoma Chuanxiong (6g), raw Radix Paeoniae Alba (9g), Fructus Forsythiae (12g), Radix Glycyrrhizae (6g), Trichosanthes kirilowii Maxim (15g) and Pericarpium Citri Reticulatae Viride (6g). All the dried herbs were purchased from Binjiang outpatient department of Zhejiang Chinese Medical University. Prescription dosage of RYF was milled into powder and soaked in 8

times prescription dosage distilled water, and then extracted with boiling water under reflux for two hours. The extract was filtered, and the extraction was repeated once. Subsequently, the filtrates were combined and evaporated under vacuum (RV8V, IKA, Werke GmbH & CO. KG, Staufen, Germany) and then lyophilized with a freeze dryer (VirTis, AD 2.0 EL, SP Scientific, USA) into powder. The percentage yield of RYF aqueous extract was 9.61% (w/w).

Chromatographic analysis was performed using C18 column (250mm × 4.6μm, 5μm; Waters) maintained 25℃. A binary mobile phase consisting of acetonitrile (A) and water-acetic acid (B; 100:0.2, v/v) was used at a flow rate of 1.0 ml/min. Gradient elution was performed according to the following elution program: 0-6 min, 10-20% A; 6-8 min, 20% A; 8-15 min, 20-23% A; 15-17 min, 23-25% A; 17-27 min, 25-50% A; 27-37 min, 50-80% A; 37-45 min, 85-10% A. The injection volumn was 10 μl and the detection wavelength was set at 284 nm. Each of the reference standards (Calycosin-7-glucoside, ferulic acid, lobetyolin, ligustilide) was dissolved in methanol to prepare the stock solution. The lyophilized powder was accurately weighted (0.109 g), then dissolved in water (1.13 g dried herbs/ml) and the solution was centrifuged at 12,000 rpm for 10 min, and the 10 μl supernatant was injected into the HPLC system for analysis.

Animals and cells

BALB/c mice (4-6 w, Female) were purchased from BK Corporation (China). All animal experiment was performed under semi-sterile conditions. The animals were stored in special-pathogen-free (SPF) environment during entire experiment. Water and food were provided normally. Animals were maintained under the standard 12 light/dark cycle at 22-23℃ with relative humidity of 50-60%. All animals' protocols were approved by the Institutional Animal Care and Use Committee at Zhejiang Chinese Medical University Laboratory Animal Research Center.

The mice breast cancer cell line (4T1), Plasmid SSR#69 (designed by Professor Westerman) and PAMPHO plasmid, were favored from Professor Tong-chuan He from the University of Chicago. LipofectAMINE 2000 was purchased from Invitrogen (California, USA). The human embryonic kidney cell 293 (HEK-293) was purchased from Cell Bank of the Chinese Academy of Sciences (Shanghai, China). Thymic epithelial cells (TECs) was obtained from BALB/c mice [19]. All of the cell lines were cultured in DMEM (Gibco, USA) containing 10 % fetal bovine serum (Gibco, USA) at 37℃ with 5% CO_2.

Mice mammary tumor model establishment

After two days of acclimatization, mice were with 100 μl of 4T1 cell suspension subcutaneously into the 2rd pair mammary fat pad on the right at a cell density of 1.0×10^7 cells/ml (the normal group were injected with a vehicle of PBS). Two days after tumor inoculation, animals (n=4) were randomly divided into five groups (four mice per group): (i) cyclophosphamide (CTX, Baxter, Shanghai, China) group (30 mg/kg, i.p. once every two days); (ii) model group (0.2 ml, intragastrically, normal saline, once a day); (iii) RYF-L (low concentration) group (0.145g crude herbs/kg, intragastrically, once a day); (iv) RYF-M (medium concentration) group (0.29g crude herbs/kg, intragastrically, once a day); (v) RYF-H (high

concentration) group (0.58g crude herbs/kg, intragastrically, once a day). Four health mice were prepared in normal group (0.2 ml, intragastrically, normal saline, once a day). All treatments lasted for 20 days. Throughout the study, body weights were monitored and the longest (L, mm) and shortest (W, mm) diameter of tumor were measured with a vernier caliper weekly. Tumor volumes (V, mm^3) were calculated with Eq. 1. Mice were sacrificed 2 hours after the last administration. The visceral weight and index of thymus, lung, spleen and lymph node were measured with Eq. 2. The anti-tumor rate were calculated with Eq. 3 after collected and weighed the tumor. Calculated the pulmonary metastasis rate according to the number and volume of nodes on the lung.

$$V=(L+W)\times L\times W\times 0.2618 \qquad (1)$$

$$\text{Visceral Index}(\%)=\frac{\text{visceral mass}(g)}{\text{body mass}(g)}\times 100\% \qquad (2)$$

$$\text{Anti-tumor Rate}(\%)=(1-\frac{\text{average tumor mass of control group}(g)}{\text{average tumor mass of experimental group}(g)})\times 100\% \qquad (3)$$

Immunohistochemical analysis

Thymus tissue sections were inflated with 4% paraformaldehyde, embedded in paraffin and cut at a thickness of 5μm. Tissue sections of each specimen were stained using hematoxylin and eosin (H&E, Sangon Biotech, Shanghai) according to a standard protocol for histopathological examination using fluorescence microscope (Axio Scope.A1, Zeiss, Germany). The pathological changes in the structure of the tissue sections in each group were evaluated. The numbers of cells in thymus cortex and medulla regions were measured using Image J. 3% hydrogen peroxide was used to block endogenous peroxidase activity at room temperature for 15 min. Subsequently, the unspecific binding sites were blocked with 5% BSA/PBA for 40 min. The sections were then incubated for overnight with primary antibody at 4°C in a humid chamber for E-cadherin (Cell Signaling Technology) and Vimentin (Cell Signaling Technology). PBS was used as negative control. The dilutions used for the primary antibodies were 1:200. The sections were subsequently incubated with rabbit anti-mouse enhanced polymer antibodies (Zsbio Co., Ltd.) at 37°C for 2 h. Then the reaction products were developed with 3, 30-diaminobenzidine (DAB), counterstained with haematoxylin, differentiated with 1% hydrochloric acid ethanol, washed with distilled water, dehydrated with graded ethanol, vitrified by xylene and sealed with neutral gum. The stained sections were observed with fluorescence microscope after the sections dried. Immunoreactivity was analyzed with Image J to evaluate the expression of proteins.

Cell proliferation analysis

The establishment and evaluation of iTECs were described in our previous literature [19]. Logarithmically grown iTECs were seeded in 96-well plates (1×10^4 /well). Cells were divided into different concentration

treatment groups of RYF extraction (100 µl of 25, 50, 100, 200, 400 µg/ml). There was no cells and only 100 µl cell cultural medium in control group. Negative control group used 100 µl of cell cultural medium with 0.1% DMSO (Sangon Biotech) replaced RYF extraction. There were three wells of cells used as repeated in each group. The cells were incubated at 37 ℃ with 5% CO_2 for 48 h. 20 µl of MTT solution (5 mg/ml, Biofrox) was then added into each well. After 4 h incubation, cell culture medium was discarded, and 150 µl of DMSO was added into each well. Plates were shaken at room temperature for 10 min. Absorbance value was measured at 570 nm using Synergy H1 Multi-Mode Microplate Reader (Bio-Tek, USA). Then calculated the inhibition rate of cell proliferation (%) with MTT assay.

Logarithmically grown iTECs cells were seeded in 24-well plates (3×10^4 /well) for 24 h. There was 100 µl of cell cultural medium with 0.1% DMSO (Sangon Biotech) added in to iTECs negative control group and different concentration treatment groups of RYF extraction (300 µl of 50, 100, 200 µg/ml). The cells were incubated at 37 ℃ with 5% CO_2 for 48 h, and then cell culture medium was discarded. 300 µl of crystal violet staining solution was added into each well and stained at room temperature for 30 min. Subsequently repeated washed with water and dried naturally and then observed the proliferation. Results were expressed as percentage of cell proliferation with respect to negative control group cells (as 100%).

TGF-β1 induced iTECs EMT

TGF-β1 was used to induce EMT of iTECs. Briefly, iTECs in logarithmic growth phase were seeded in 24-well plates (3×10^4 /well) for 24 h, and then starved with serum-free medium for 24 h. Cells were divided into five groups: (i) normal group (DMED high sugar medium); (ii) TGF-β1 group (10 ng/ml TGF-β_1); (iii) RYF-L group (50 µg/ml RYF extraction and 10 ng/ml TGF-β_1); (iv) RYF-M group (100 µg/ml RYF extraction and 10 ng/ml TGF-β1); (v) RYF-H group (200 µg/ml RYF extraction and 10 ng/ml TGF-β1). There were three wells of cells used as repeated in each group. The TGF-β1 was administered first, then after 48 h the RYF extraction were added and cultured for 24 h. The morphology of iTECs cells induced by TGF-β1 was observed with microscope. The phenotype marker of E-cadherin, Vimentin and a-Tubulin was observed by immunofluorescence staining method described in 2.7. Quantitative real-time PCR analysis detected the expression level of Zeb-1 and Snail 1 and other mRNA for phenotypic markers and phenotype-related transcription factors.

Immunofluorescence staining

The cells were seeded on 24-well plates (3×10^4 /well) for 24 h and were repeated washed with PBS respectively. The sterile coverslips with cells were fixed in 4% paraformaldehyde (PFA) for 15 min. Then performed with Triton-100 (Beyotime), and blocked with 0.5% bovine serum albumin (BSA, Biofrox) for 40 min at room temperature. The cells were incubated with primary antibody, rabbit anti-mouse CK5 (1:100, Affinity), rabbit anti-mouse CK8 (1:100, Abcam) or FITC-rabbit anti-mouse E-cadherin (1:200, BD Pharmingen), rabbit anti-mouse a-Tubulin (1:100, Abcam), rabbit anti-mouse Vimentin (1:100, Cell Signaling) for overnight at 4℃. The cells were followed by incubation with secondary antibodies, FITC-

mouse anti-rabbit IgG (1:100, Santa Cruz) and PE-Goat Anti-Mouse IgG (1:100, Thermo) at room temperature for 2 h. Cell nuclei were stained with Hoechst 33258 (1 μg/ml, sigma) for 5 min. The labeled section were viewed with fluorescence confocal microscopy (Zeiss, Germany).

Quantitative Real-time Pcr Analysis

The cells were seeded on 6-well plates (1×10^5 /well) for 24 h respectively. The steps of total RNA extraction, reverse transcription, and fluorescence quantitative detection of SV40 mRNA was as described [19]. Trizol Reagent (Thermo); First Strand cDNA Synthesis Kit (Sangon Biotech). PCR amplification was performed with GAPDH as a reference to detect the expression of target mRNA by the $2^{-\Delta\Delta Ct}$ method in different group cells. There were three wells of cells used as repeated in each group. The primer sequences were listed in Table 1. Primer synthesis was performed by Shanghai Sangon.

Table 1
Sequences of primer pairs for quantitative real-time PCR.

Gene name	Forward primers (5' – 3')	Reverse primers (5' – 3')
GAPDH	GGCTGCCCAGAACATCAT	CGGACACATTGGGGGTAG
SV40	TCTTCGTCT CCG GCT CTG	CTGGCAACTTCATGCAAA
Snail 1	GTCCAGCTGTAACCATGCCT	TGTCACCAGGACAAATGGGG
E-cadherin	CAGCCGGTCTTTGAGGGATT	TGACGATGGTGTAGGCGATG
Vimentin	GGATCAGCTCACCAACGACA ACAAGCGAGAGGATCATGGC	AAGGTCAAGACGTGCCAGAG
Zeb 1		CTGCTTTCTGCGCTTACACC
Smad 2	CCAGTTGTGAAGAGACTGCT	CGGAGGAGAGCAGAATGGGC

Luciferase Analysis

Logarithmically grown iTECs cells were seeded in 24-well plates (3×10^4 /well) until the cell density reached 80%-90%. Then discarded the culture medium, washed by serum-free DMEM, added 1.2-2.0 ml serum-free DMEM and put in the culture incubator for 20 min. The pBGLuc-Smad plasmid was infected and transfected by LipofectAMINE 2000. Subsequently, the successful infection and transfection iTECs were divided and treated by the method described in 2.8. The luciferase level of all groups cell supernatant liquid (50 μl) were analyz ed with single-channel bioluminescent detector according to the Luciferase gene kit's instruction and calculated the relative activation degree of Smad pathway (%). The expression of Smad mRNA of each group was detected by PCR.

Statistical Analysis

The statistical analysis was performed with SPSS 20.0 software and the results were expressed as mean ± SD. One way ANOVA were used to compare means of multiple groups and least significant difference test was used for comparison between two groups. Differences were considered to be statistically significant when $P < 0.05$.

Results

HPLC analysis of RYF extract

Four components were analyzed and determined by HPLC by comparing with the referenced solution. In Fig. 1, No. 15 peak was calycosin-7-glucoside, No. 19 peak was ferulic acid, No. 20 peak was lobetyolin, and No. 29 peak was ligustilide. The concentration were 1.3 mg/g, 0.11 mg/g, 0.12 mg/g and 0.015 mg/g in dried herbs, respectively.

Anti-tumor Effects Of Ryf In Mammary Tumor Model Mice

Figure 2 showed the thymus, lung, spleen, lymph node and tumor index in mammary tumor model mice increased significantly compared with normal group. Compared with model group, the spleen, thymus and tumor index in CTX group decreased significantly, and the anti-tumor rate was 51.33%. In addition, a notable decrease of spleen index in RYF-L group and tumor index in RYF-M and RYF-H group compared with model group, and the anti-tumor rate in RYF-L, RYF-M and RYF-H were 6.49%, 31.43% and 33.45%, respectively.

As showed in Table 2 and Fig. 2G, compared with model group, both of the number of pulmonary metastasis (diameter > 2 mm and < 2 mm) in CTX and RYF treated groups reduced significantly. The pulmonary metastasis rate in model group was 100%, and in CTX group, low, medium and high concentration RYF was 50%, 75%, 75% and 100%, respectively.

Table 2
The number of pulmonary metastasis (diameter > 2 mm and < 2 mm) and pulmonary metastasis rate in different groups. The data shows as the mean ± SD (n=4). *P<0.05, **P<0.01 compared to the model group.

Group	Number of pulmonary metastasis	Diameter > 2 mm	Diameter < 2 mm	Pulmonary metastasis rate
Model group	3.25 ± 0.25	1.50 ± 0.58	1.75 ± 0.50	4/4
RYF-L group	1.00 ± 0.82**	0.50 ± 0.58*	0.50 ± 0.58**	3/4
RYF-M group	1.25 ± 0.96**	0.25 ± 0.50*	1.00 ± 1.16	3/4
RYF-H group	1.75 ± 0.50**	0.50 ± 0.58*	1.25 ± 0.50	4/4
CTX group	0.50 ± 0.58**	0.25 ± 0.50*	0.25 ± 0.50**	2/4

RYF altered histomorphology of thymus in mammary tumor model mice

It was clear-out of the thymus cortex and medulla boundaries and cells had a regular arrangement in normal group (Fig. 3A). Meanwhile, the cortex regions had darker staining, indicate it has more thymocytes than medulla regions. On the contrary, the boundaries between thymus cortex and medulla were indistinct and the cells arranged disordered in model group with cortex regions cells reducing notably and medulla regions cells increasing remarkably compared to normal group. In addition, CTX and RYF-treated groups all had clear boundaries between thymus cortex and medulla. Moreover, the cells in cortex increased significantly and in medulla cells decreased notably compared with model group as seen in Fig. 3B.

RYF influenced the expression of E-cadherin and Vimentin in thymus tissue

E-cadherin is the characteristic markers of epithelial cells and Vimentin is the interstitial cells. The E-cadherin positive cells in model group reduced significantly and Vimentin positive cells increased notably compared with normal group (Fig. 4A). Conversely, compared to the model group, the cells with E-cadherin positive expression increased and with Vimentin positive expression reduced in RYF-treated groups and CTX group. (Fig. 4B).

Ryf Promoted Proliferation Of Itecs

MTT assay results showed that RYF treatment promoted the proliferation of iTECs (Fig. 5A). The cell proliferation rate of RYF-treated groups (100, 200, 400 μg/ml) increased significantly compared with control group in a dose-dependent manner. Crystal violet staining experiment also suggested RYF-treated groups (100, 200 μg/ml) promoted the proliferation of iTECs (Fig. 5B).

Ryf Altered Morphology Of Itecs After Tgf-β1 Treatment

The morphology observation (Fig. 5C) results showed iTECs were short fusiform and lined up tightly in normal group. Besides, the number of iTECs induce by TGF-β1 reduced and intercellular spaces got fewer with the morphology changed to long fusiform. Simultaneously, RYF treated could reverse the change of intercellular space and morphology.

RYF influenced the mRNA levels and protein expressions of E-cadherin, Vimentin, Snai1 and Zeb1 in TGF-β1 induced iTECs

Compared with normal group, the E-cadherin's expression and mRNA's level decreased and Vimentin's expression and mRNA's level were up-regulation in TGF-β1 group. Moreover, the level of Snail 1 and Zeb 1 increased significantly. Furthermore, compared with TGF-β1 group, RYF-treated groups reversed the change in relative proteins expression and mRNA levels. The results showed in Fig. 6A, B, C and D.

As seen in Fig. 6E, F, G, immunofluorescence staining results showed the target proteins presented in green fluorescence and the cell nucleus presented in blue. TGF-β1 group and RYF-M group' α-Tubulin fluorescent expression results suggested that RYF could resist the change of the TGF-β1-induced iTECs' morphology and could maintain normal cell morphology.

Ryf Affected Smad Pathway

As showed in Fig. 7, PCR results suggested that the level of Smad mRNA was up-regulated significantly compared to the normal group in iTECs after TGF-β1 induced. Interestingly, the level of Smad2 mRNA was down-regulated after RYF treated compared to the TGF-β1 group and differences were considered to be statistically significant (P<0.01).

Luciferase assay results showed the expression of luciferase increased significantly in TGF-β1 group compared to the normal group, and it indicated that Smad pathway got activated. Furthermore, the luciferase expression in RYF-treated groups were down-regulated. The difference between RYF-L and TGF-β1 group were considered to be statistically significant (P<0.05).

It was reported that the activation of Smad pathway could induce the phenomenon of cell type II EMT [20]. Moreover, it is suggested that RYF can be confronted the phenotypic transition of iTECs induced by TGF-β1. This change may be caused by TGF-β1 activation of the Smad pathway and induced thymic epithelial cell type II EMT.

Discussion

Our research found that the tumor index and lung metastases of RYF was significantly lower while compared with the model group (P < 0.05). Moreover, the boundary between medulla and cortex in mouse thymus in RYF was clearer, and the cell number was significantly increased in cortical area and decreased in medulla area than that in the model group. RYF could increase the expression of E-cadherin and

decrease Vimentin in vivo. The above results were confirmed by cell experiments, after induced with TGF-β1, the mRNA levels of Smad was up-regulated, after treatment with RYF, the mRNA levels of Smad were down-regulated, and the activation of signaling pathways was inhibited. It is suggested that RYF could confront the phenotypic transition of iTECs induced by TGF-β1, and its mechanism is related to the inhibition of Smad pathway.

As an important part of prescription, the Radix Codonopsis, Astragalus membranaceus and Angelica Sinensis in RYF have better therapeutic effects in improving immune and anti-tumor. As one of the most important immune organs, the abnormal changes of thymus usually use to evaluate body's immune function. The findings and results of this study indicated that the thymus index of tumor-bearing mice increased slightly but the pathological changes of thymus were reduced noticeably after RYF treated, what reminded RYF could repair the thymus function of tumor-bearing body and played an important role in adjuvant or combination therapy of advanced breast cancer.

The TGF-β coordinates essential cellular functions, including proliferation, differentiation and morphogenesis [21]. Many breast cancer cells, especially 4T1, secrete high levels of TGF-β1 [22]. Consequently, TGF-β has been widely used to induce phenotypic changes of epithelial cells, and mediates the transformation of epithelial cells into mesenchymal cells, thus inhibiting the migration of tumor cells.

As an important development process of cell adhesion and migration during tumor invasion, the hallmarks of EMT is the functional loss of E-cadhetrin [23, 24]. E-cadherin is one of cadherin members, which is a calcium-dependent cell adhesion molecule of the epithelial cells, maintains the epithelial tissues but also plays a pivotal role in organogenesis and morphogenesis [25]. Vimentin is an intermediate filament characteristically present only in certain epithelial of mesenchymal cells [26]. In general, E-cadherin is the epithelial marker and Vimentin is regarded as the mesenchymal marker. Gain of Vimentin and loss of E-cadherin is a hallmark of EMT and E-cadherin is a good prognostic marker whereas Vimentin expression indicates a poor prognosis [27]. This study showed RYF therapy could effectively reverse the cell morphology changes and the abnormal expression of E-cadherin and Vimentin in TGF-β1-induced iTECs, what suggested RYF could confront the TGF-β1-induced EMT in iTECs.

EMT is regulated by several transcription factors, including Snail and Zeb, which downregulate E-cadherin expression [28]. As two key transcription factors for cell motility, Snail and Zeb trigger EMT by repression of epithelial markers and activation of mesenchymal properties. This study showed the expression of Snai1 and Zeb1 in TGF-β1-induced iTECs increased while they reduced after RYF treated and then inhibited EMT. It also adds to the proof that RYF could confront the TGF-β1-induced EMT in iTECs.

Smad signaling pathways are necessary for EMT[29], and TGF-β could induce EMT in NMuMG cells through activation of Smad, while in renal tubular epithelial cells, non-Smad pathways can not be activated of EMT-related transcription factors[30, 31]. Our study results showed Smad pathway got activated in the phenotypic transition process of TGF-β1-induced iTECs. Meanwhile, the expression of Smad luciferase and level of mRNA reduced after RYF treated, which suggested TGFβ1-induced thymic epithelial cell EMT through activation of the TGFβ/Smad pathway of RYF.

Conclusion

The thymic function of the tumor-bearing body was markedly abnormal, which was mainly due to the disorder of cortex and medulla regions cells and atrophy of the medulla. Interestingly, RYF could reverse the phenotypic changes of TECs by inhibiting TGF-β1-induced Smad pathway, and down-regulation expression of Snail 1 and Zeb 1, and then inhibited the transformation from epithelial cells to mesenchymal cells. It means that RYF can help to repair the thymus function of tumor-bearing mice and plays a role in treatment of breast cancer, and the mechanism may be related to inhibit the TGF-β1-induced EMT of thymic epithelial cell through Smad pathway.

Abbreviations

Abbreviations

RYF: Ruyong Formula; TEC: thymus epithelial cells; iTEC: immortalized thymus epithelial cells; HPLC: high performance liquid chromatography; MTT: 3-(4,5-dimethylthiazol-2-yl)-2,5-diphenyltetrazolium bromide; TGF-β1: transforming growth factor-β1; EMT: epithelial–mesenchymal transition; CTX: Cyclophosphamide.

Declarations

Acknowledgements

We appreciate the great technical support from the Public Platform of Pharmaceutical Research Center, Academy of Chinese Medical Science, Zhejiang Chinese Medical University.

Authors' Contributions

JL Gao (jianligao@zcmu.edu.cn) and K He (116310366@qq.com) conceived and designed the project. BQ He, RZ Shi, QH L, WQ Guo and X Xu completed the experiments and wrote the manuscript.

Funding

The study was supported by a grant from National Natural Science Foundation of China (No. 81473575), Natural Science Foundation of Zhejiang Province of China (No. LY19H280010) and Public Welfare Technology Research Program of Zhejiang Province of China (No. LGC20B050010). Opening Project of Zhejiang Provincial Preponderant and Characteristic Subject of Key University (Traditional Chinese Pharmacology) to Zhejiang Chinese Medical University (No. ZYAOX2018015), university project of Zhejiang Chinese Medical University (No. 2019ZG50), Young and Middle-aged Scientific Research and Innovation Fund Projectof Zhejiang Chinese MedicalUniversity (No.KC201916).

Availability of data and materials

The data used to support the findings of this study are available from the corresponding author upon request.

Ethics approval and consent to participate

All procedures were performed in accordance with the guidelines of the Zhejiang Chinese Medical University ethics committee.

Consent for publication

Not applicable.

Competing interests

All authors declare that there is no duality of interest associated with this manuscript.

Author details

[1] Zhejiang Chinese Medical University, Hangzhou, Zhejiang 310053, China. [2] Tangqi Branch of Traditional Chinese Medicine Hospital of Yuhang District, Hangzhou, Zhejiang 311106, China. [3] The First Affiliated Hospital, School of Medicine, Zhejiang University, Hangzhou, Zhejiang 310009, China.

References

1. Anastasiadi Z, Lianos GD, Ignatiadou E, et al. Breast cancer in young women: an overview. Updates in Surg. 2017;69:313–7.
2. Chen Y, Chen L, Zhang JY, et al. Oxymatrine reverses epithelial-mesenchymal transition in breast cancer cells by depressing αvβ3 integrin/FAK/PI3K/Akt signaling activation. Onco Targets Ther. 2019;12:6253–65.
3. Qi F, Zhao L, Zhou A, et al. The advantages of using traditional Chinese medicine as an adjunctive therapy in the whole course of cancer treatment instead of only terminal stage of cancer. Biosci Trends. 2015;9(1):16–34.
4. Fukutake M, Yokota S, Kawamura H, et al. Inhibitory effect of Coptidis Rhizoma and Scutellariae radix on azoxymethane-induced aberrant crypt foci formation in rat colon. Biol Pharm Bull. 1998;21:814–7.
5. Qin N, Lu S, Chen N, et al. Yulangsan polysaccharide inhibits 4T1 breast cancer cell proliferation and induces apoptosis in vitro and in vivo. Int J Bio Macromol. 2019;121(10):971–80.
6. Wang W, Chen B, Zou RL, et al. Codonolactone, a sesquiterpene lactone isolated from Chloranthus henryi Hemsl, inhibits breast cancer cell invasion, migration and metastasis by downregulating the transcriptional activity of Runx2. Int J Oncol. 2014;45(5):1891–900.
7. Kim YJ, Lee JY, Kim HJ, et al. Anti-Inflammatory Effects of Angelica sinensis (Oliv.) Diels Water Extract on RAW 264.7 Induced with Lipopolysaccharide. Nutrients. 2018;10(5):647–58.

8. Zhou R, Chen H, Chen J, et al. Extract from Astragalus membranaceus inhibit breast cancer cells proliferation via PI3K/AKT/mTOR signaling pathway. BMC Complement Altern Med. 2018;18(1):83–90.
9. Oliveira CR, Spindola DG, Garcia DM, et al. Medicinal properties of Angelica archangelica root extract: Cytotoxicity in breast cancer cells and its protective effects against in vivo tumor development. J Integr Med. 2019;17(2):132–40.
10. Zhou L, Liu Z, Wang Z, et al. Astragalus polysaccharides exerts immunomodulatory effects via TLR4-mediated MyD88-dependent signaling pathway in vitro and in vivo. Sci Rep. 2017;7(1):44822–34.
11. Ke XQ, Wang S, Fu JJ, et al. The natural compound codonolactone attenuates TGF-beta 1-mediated epithelial-to-mesenchymal transition and motility of breast cancer cells. Oncol Rep. 2016;35(1):117–26.
12. Ye Q, Su L, Chen D, et al. Astragaloside IV Induced miR-134 Expression Reduces EMT and Increases Chemotherapeutic Sensitivity by Suppressing CREB1 Signaling in Colorectal Cancer Cell Line SW-480. Cell Physiol Biochem. 2017;43(4):1617–26.
13. Zhu J, Wen K. Astragaloside IV inhibits TGF-β1-induced epithelial–mesenchymal transition through inhibition of the PI3K/Akt/NF-Kb pathway in gastric cancer cells. Phytother Res. 2018;32(7):1289–96.
14. Chiu SC, Chiu TL, Huang SY, et al. Potential therapeutic effects of N-butylidenephthalide from Radix Angelica Sinensis (Danggui) in human bladder cancer cells. BMC Complement Altern Med. 2017;17(1):523–34.
15. Wang Z, Liu Z, Yu G, et al. Paeoniflorin Inhibits Migration and Invasion of Human Glioblastoma Cells via Suppression Transforming Growth Factor β-Induced Epithelial–Mesenchymal Transition. Neurochem Res. 2018;43(2):760–74.
16. Zhang Y, Miao H, Yan H, et al. Hepatoprotective effect of Forsythiae Fructuse water extract against carbon tetrachloride-induced liver fibrosis in mice. J Ethnopharmacol. 2018;218(3):27–34.
17. Song L, Xu X, Li Z. A serine protease extracted from Trichosanthes kirilowii inhibits epithelial-mesenchymal transition via antagonizing PKM2-mediated STAT3/Snail1 pathway in human colorectal adenocarcinoma cells. J Funct Foods. 2018;40(1):639–47.
18. Shi RZ, Shen JM, Zhang JY, et al. Effects and mechanisms of Ruyong Formula on phenotypic changes of thymic epithelial cells in 4T1 breast cancer mice. Academic Journal of Shanghai University of Traditional Chinese Medicine. 2020;34(1):45–56.
19. Shen JM, Ma L, He K, et al. Identification and functional study of immortalized mouse thymic epithelial cells. Biochem Biophys Res Commun. 2020;525(2):440–6.
20. Ko H, So Y, Jeon H, et al. TGF-β1-induced epithelial-mesenchymal transition and acetylation of Smad2 and Smad3 are negatively regulated by EGGG in Human A549 lung cancer cells. Cancer Lett. 2013;355(1):205–13.
21. Toomer KH, Malek TR. Cytokine Signaling in the Development and Homeostasis of Regulatory T cells. Cold Spring Harb Perspect in Biol. 2018;10(3):a028597.

22. Zhang F, Dong W, Zeng W, et al. Naringenin prevents TGF-β1 secretion from breast cancer and suppresses pulmonary metastasis by inhibiting PKC activation. Breast Cancer Res. 2016;18(1):38.
23. Peinado H, Olmeda D, Cano A. Snail. ZEB and bHLH factors in tumour progression: an alliance against the epithelial phenotype? Nat Rev Cancer. 2007;7(6):415–28.
24. Gloushankova NA, Zhitnyak IY, Rubtsova SN. Role of epithelial-mesenchymal transition in tumor progression. Biochemistry. 2018;83:1469–76.
25. Florescu A, Mărgăritescu C, Simionescu CE, et al. Immunohistochemical expression of MMP-9, TIMP-2, E-cadherin and vimentin in ameloblastomas and their implication in the local aggressive behavior of these tumors. Rom J Morphol Embryol. 2012;53(4):975–84.
26. Fraga CH, True LD, Kirk D. Enhanced expression of the mesenchymal marker, vimentin, in hyperplastic versus normal human prostatic epithelium. J Urol. 1998;159(1):270–4.
27. Akhtar K, Ara A, Siddiqui S, et al. Transition of Immunohistochemical Expression of E-Cadherin and Vimentin from Premalignant to Malig. Oman Med J. 2016;31(3):165–9.
28. Veloso ES, Gonçalves I N N, Silveira TL, et al. ZEB and Snail expression indicates epithelial-mesenchymal transition in canine melanoma. Res Vet Sci. 2020;131:7–14.
29. Damian M, Elizabeth DH, Daniel AG. Cooperation between Snail and LEF-1 Transcription Factors Is Essential for TGF-β1-induced Epithelial-Mesenchymal Transition. Mol Biol Cell. 2006;17(4):1871–9.
30. Piek E, Moustakas A, Kurisaki A, et al. TGF-(beta) type I receptor/ALK-5 and Smad proteins mediate epithelial to mesenchymal transdifferentiation in NMuMG breast epithelial cells. J Cell Sci. 1999;112(24):4557–68.
31. Sato M, Muragaki Y, Saika S, et al. Targeted disruption of TGF-beta1/Smad3 signaling protects against renal tubulointerstitial fibrosis induced by unilateral ureteral obstruction. J Clin Invest. 2003;112(10):1486–94.

Figures

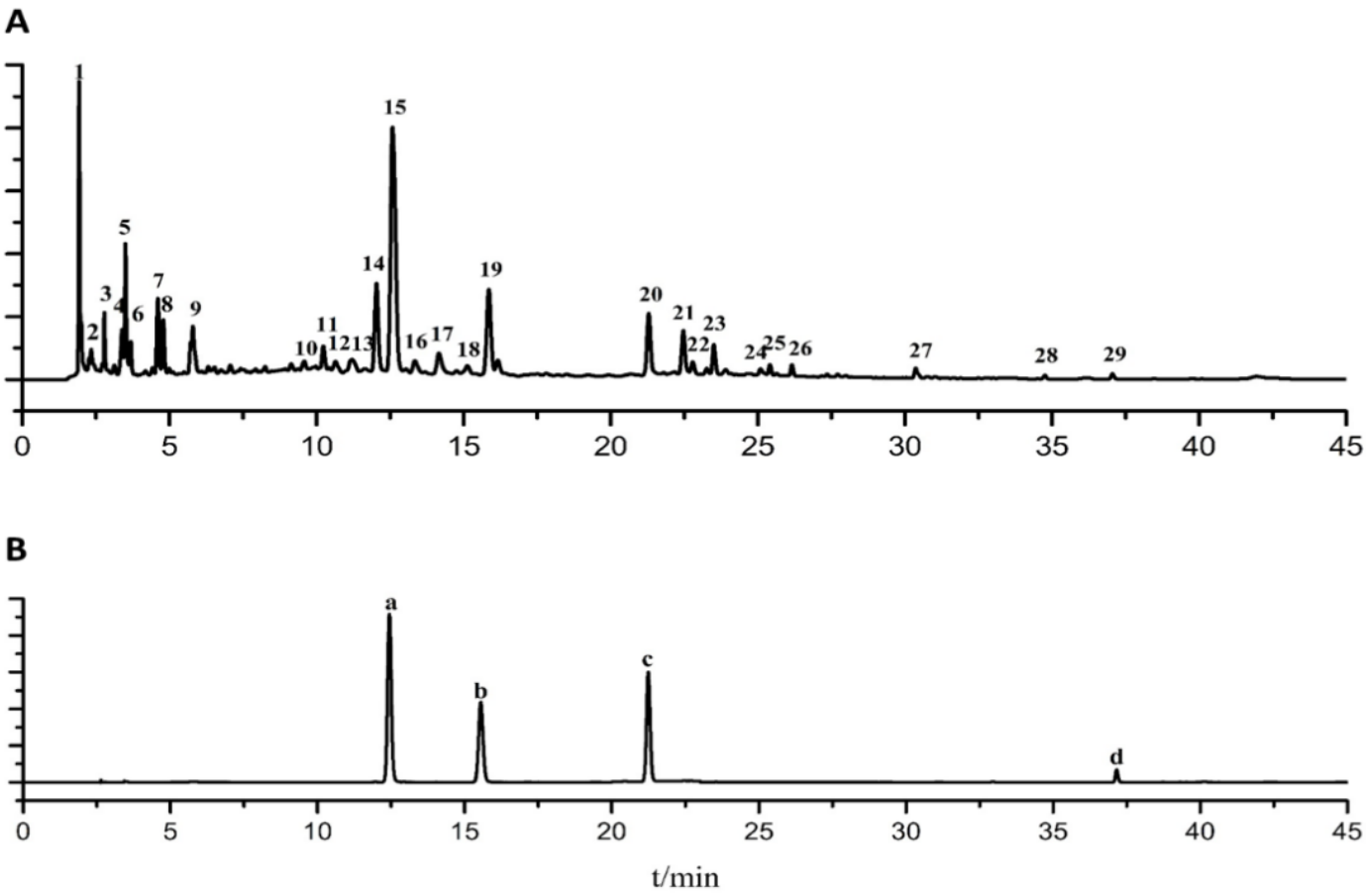

Figure 1

The HPLC chromatogram of RYF and standard references solution. (A) RYF fingerprint. (B) References: a. calycosin-7-glucoside; b. ferulic acid; c. lobetyolin; d. ligustilide.

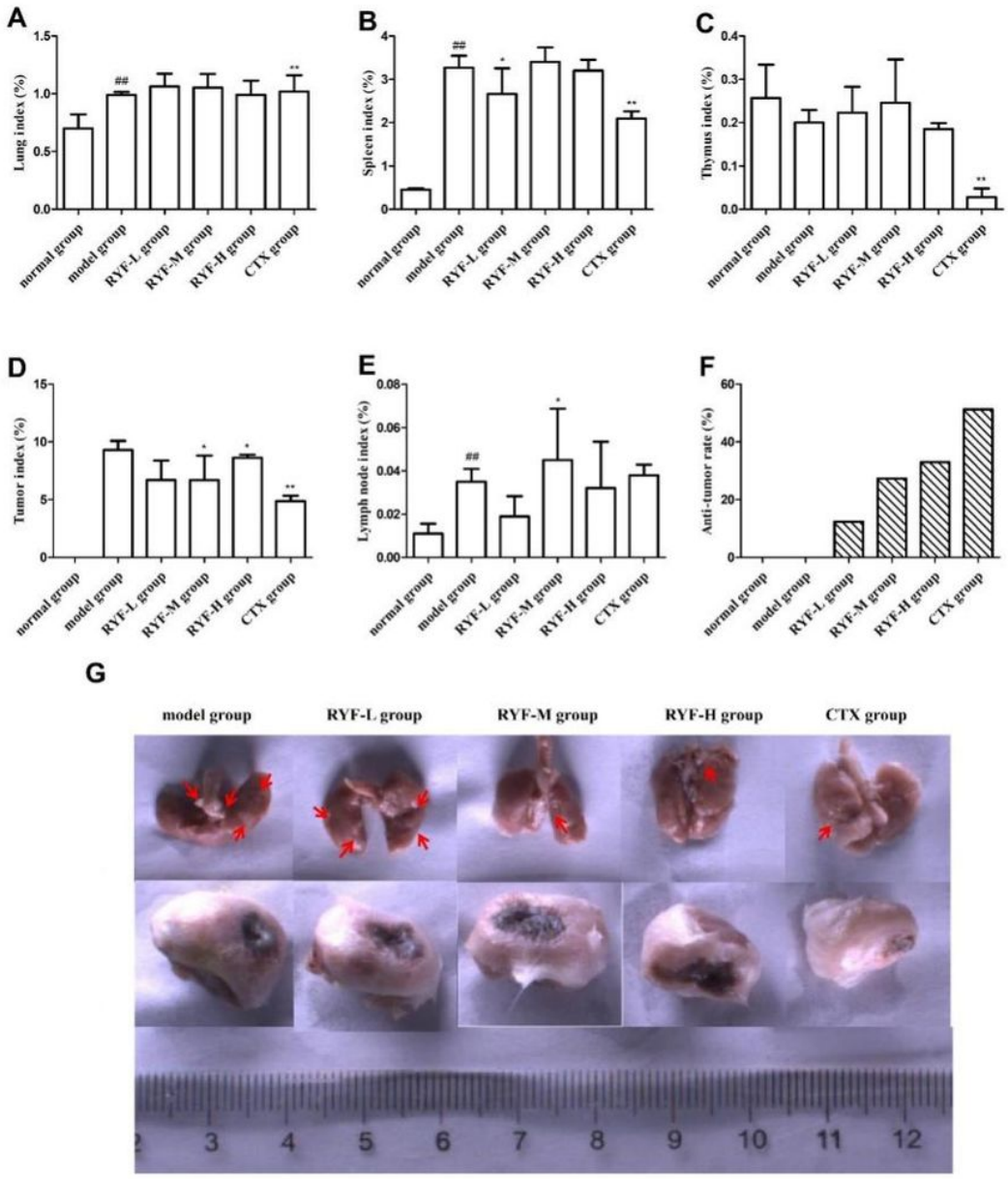

Figure 2

The organ index of lung (A), spleen (B), thymus (C), lymph node (D), tumor index (E) and auti-tumor rate (F) and effects of different groups changes on organs of BALB/c mice (lung and tumor tissue) (G) in mice of different groups. The data except anti-tumor rate are presented as the mean ± SD (n=4). #P<0.05, ##P<0.01 compared to the normal group. *P<0.05, **P<0.01 compared to the model group.

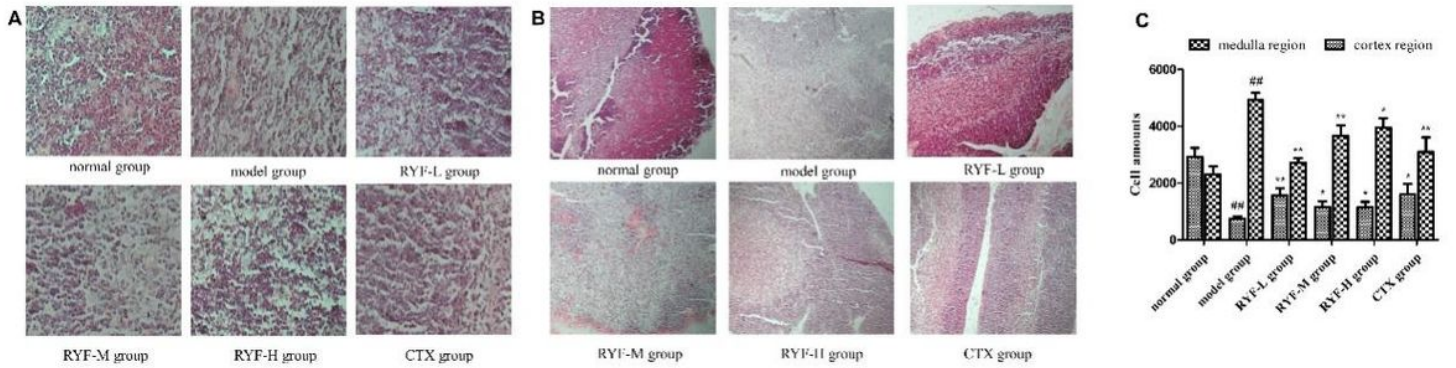

Figure 3

Changes of histomorphology in mammary tumor model mice. (A and B) Representative thymus histomorphology section of mice in different groups (A: Magnification: 200×; B: Magnification: 100×). (C) The cells in cortex and medulla regions in different groups. The data are presented as the mean ± SD (n=4). #P<0.05, ##P<0.01 compared to the normal group. *P<0.05, **P<0.01 compared to the model group.

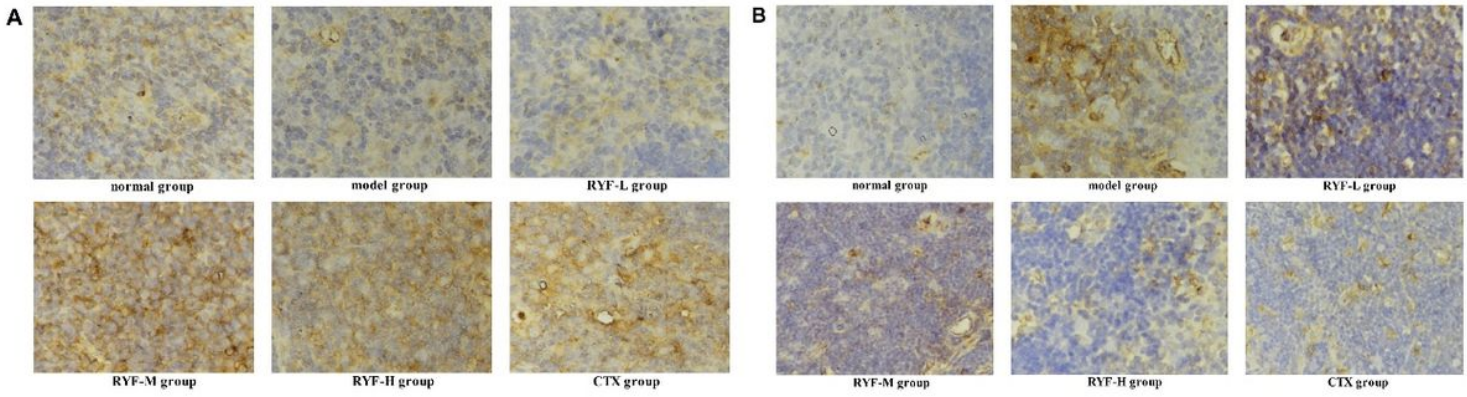

Figure 4

The expression of E-cadherin (A) and Vimentin (B) in thymus tissue. (Magnification: 100×)

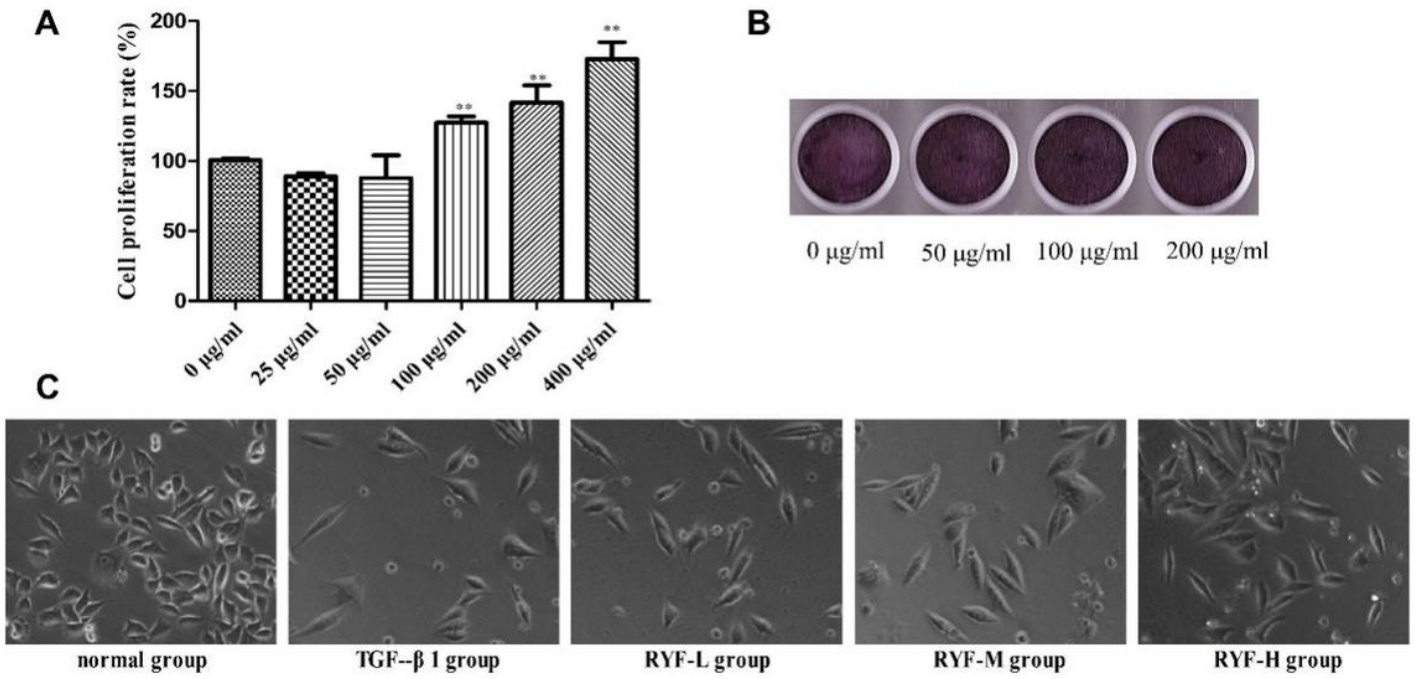

Figure 5

The proliferation of iTECs after RYF treated. (A) iTECs proliferation rate after treated by different concentration of RYF. The data are presented as the mean ± SD (n=3). *P<0.05, **P<0.01 compared to the 0 μg/ml group. (B) Cell proliferation images of crystal violet staining experiment (Magnification: 200×). (C) Cell morphology images of iTECs in different groups for 48 h (Magnification: 200×).

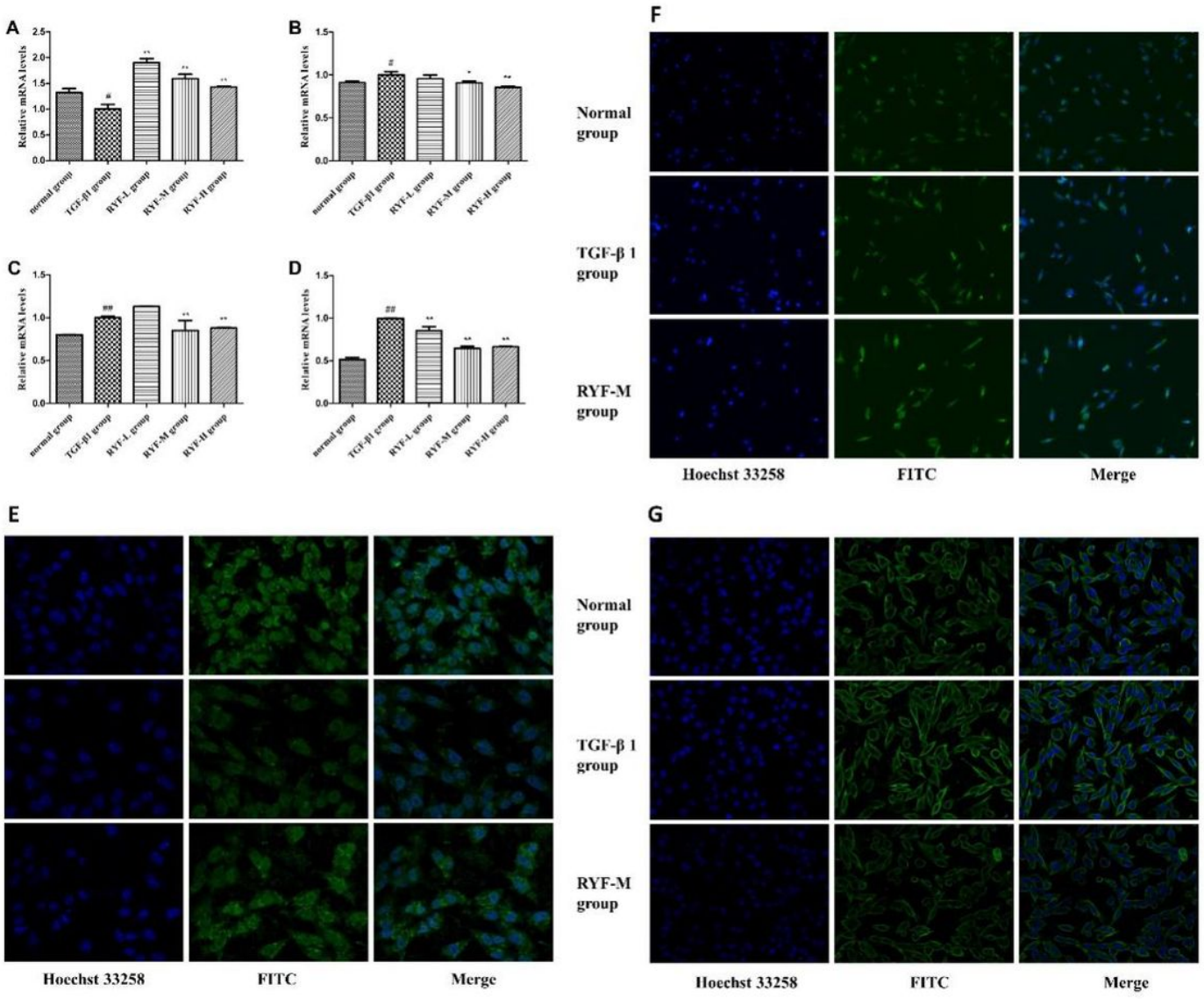

Figure 6

The mRNA levels of E-cadherin (A), Vimentin (B), Snail 1 (C) and Zeb 1 (D) in iTECs of different groups. Immunofluorescence staining section of E-Cadherin (E), Vimentin (F) and β-Tubulin (G) protein expression of iTECs in different groups (Magnification: 200×). The data are presented as the mean ± SD (n=3). #P<0.05, ##P<0.01 compared to the normal group. *P<0.05, **P<0.01 compared to the TGF-β1 group.

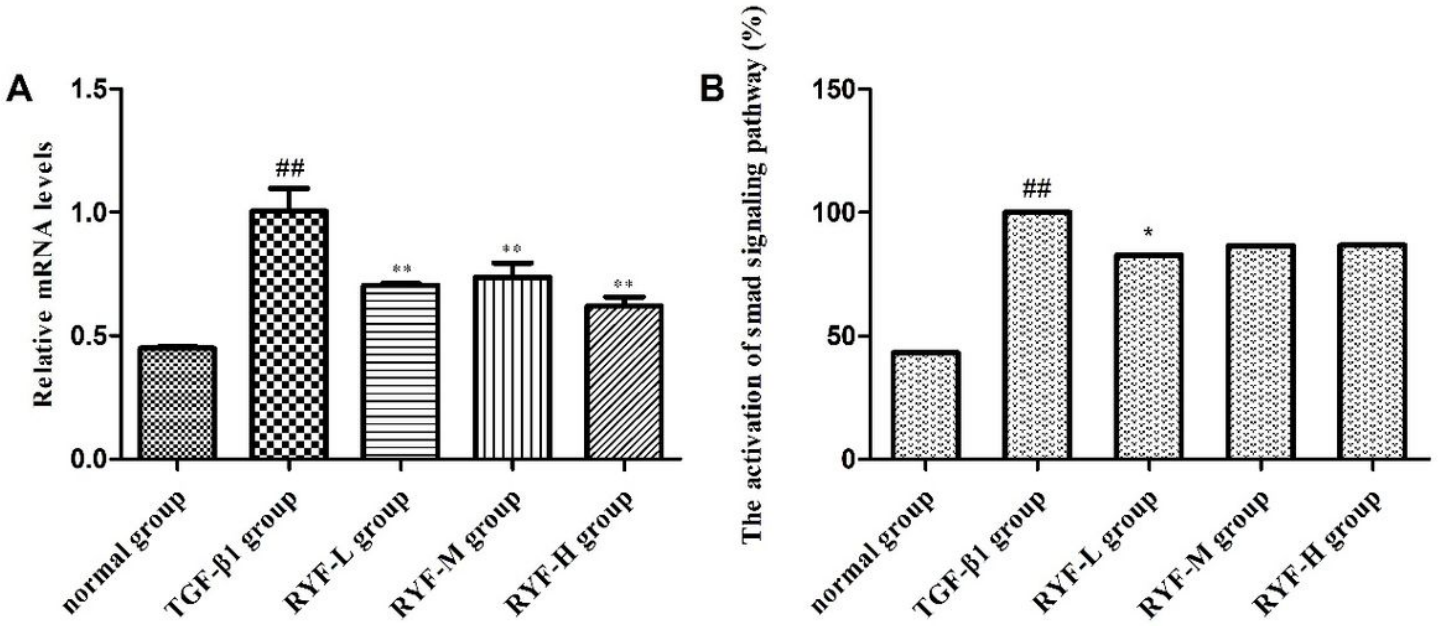

Figure 7

(A) The mRNA expression of Smad2 in iTECs of different groups. (B) Luciferase gene detection results of iTECs. The data are presented as the mean ± SD (n=3). #P<0.05, ##P<0.01 compared to the normal group. *P<0.05, **P<0.01 compared to the TGF-β1 group.